# A Traction Force Threshold Signifies Metastatic Phenotypic Change in Multicellular Epithelia

Yao Zhang[1], Xuechen Shi[2], Tiankai Zhao[1], Changjin Huang[1], Qiong Wei[1], Xin Tang[3], Lorraine C. Santy[4], M. Taher A. Saif[5], Sulin Zhang[1,2,*]

[1]Department of Engineering Science and Mechanics, The Pennsylvania State University, University Park, PA 16802, USA
[2]Department of Biomedical Engineering, The Pennsylvania State University, University Park, PA 16802, USA
[3]Department of Mechanical and Aerospace Engineering, University of Florida, Gainesville, Florida 32611, USA
[4]Department of Biochemistry and Molecular Biology, The Pennsylvania State University, University Park, PA 16802, USA
[5]Department of Mechanical Science and Engineering, The University of Illinois, Urbana, IL 61801

*To whom correspondence should be addressed. E-mail: S. Z. (suz10@psu.edu)

## Supplementary materials and methods

**Immunofluorescence**. For E-cadherin and FAK staining, cells were fixed with 4% paraformaldehyde, permeabilized with 0.1% Triton X-100, blocked with Image-iT FX signal Enhancer (Invitrogen) and sequentially incubated with primary and secondary antibodies. Mouse primary antibody anti-E-Cadherin (Invitrogen) and Alexa Fluor® 488 goat anti-mouse IgG (H+L, 495/519, green) (Invitrogen) were used for staining E-cadherin. Purified Mouse Anti-Human FAK (pY397) (BD Biosciences) and Alexa Fluor® 488 goat anti-mouse IgG (H+L, 495/519, green) (Invitrogen) were used for staining FAK. For live/dead staining, cells were fixed with 4% paraformaldehyde and then incubated with LIVE/DEAD Viability Kit (Invitrogen).

**Real-time recording of cell dispersion from a cohesive HCT-8 colony.** HCT-8 cells were cultured on 20.7 kPa gels in an incubator until day 7 and then moved to an environmental chamber for live-cell imaging. Cell dispersion dynamics from a cohesive HCT-8 colony within 10 hours was recorded at day 7 of culture.

**Preparation of polyacrylamide substrates for traction force microscopy.** PAA gels bound to coverslips were prepared using the protocol developed by Wang *et al*[1]. PAA gel stiffness was

controlled by varying bis-acrylamide and acrylamide concentrations[2]. To track the deformation of PAA gel caused by the extracellular traction, fluorescent beads (0.2 μm in diameter, Invitrogen) were embedded in a single plane near PAA gel surface, rather than uniformly embedded in the gel thickness in conventional traction force microscopy. Briefly, a glass slide was sequentially coated with Poly-D-Lysine and fluorescent beads. Pre-polymerization PAA hydrogel solution was sandwiched between the glass slide and an amino-silanized coverslip. During polymerization, the fluorescent beads coated on glass slide surface were transferred into the gel. After polymerization, the glass slide was removed and the fluorescent beads were left in the gel and located at the subsurface of the PAA gel (about 0.2 μm from the top surface of the gel). PAA gels were activated using hydrazine hydrate (Acros Organics) and then coated with 50 μg/ml ECM protein fibronectin (Sigma) for one hour. HCT-8 cells (ATCC) were cultured on PAA gels in RPMI-1640 medium (ATCC) supplemented with 10% (v/v) horse serum (ATCC) and 0.1% (v/v) penicillin-streptomycin (Invitrogen).

Tang *et. al.* have prepared PAA gels with different stiffness from different relative concentration of acrylamide and bis-acrylamide solution, and measured their Young's moduli using atomic force microscopy (AFM)[3]. We followed this work to prepare PAA gels with different stiffness. The relative concentration of acrylamide and bis-acrylamide and resulting gel moduli are as follows[3]: 2.6±0.2 kPa PAA gel (4% acrylamide and 0.15% bis-acrylamide); 4.5±1.2 kPa PAA gel (5% acrylamide and 0.15% bis-acrylamide); 20.7±1.0 kPa PAA gel (8% acrylamide and 0.13% bis-acrylamide); 47.1±1.9 kPa PAA gel (8% acrylamide and 0.48% bis-acrylamide).

**Traction force microscopy (TFM).** TFM involves two basic steps: measuring the displacement field of a compliant substrate due to the traction force and inversely mapping out the traction force distribution from the displacement field by elasticity theories. Fluorescent beads on the substrate surface serve as tracers of substrate deformation. To obtain the displacement field, a pair of images of the beads on the subsurface of the substrate, taken before and after detaching cells, is recorded using fluorescent microscopy. The optical flow of two images is analyzed by particle image velocimetry (PIV), giving rise to the in-plane displacement field of the subsurface. The displacement field of the free surface can be approximated to be that of the subsurface because of their nanometer closeness. Since the thickness of substrate is typically much larger

than the displacement caused by cell traction, the substrate can be considered as an elastic and half-space medium. The traction force field can be constructed by solving an inverse problem based on Boussinesq solution[4-7].

In our TFM, the fluorescent beads are embedded on a single plane underneath the surface. This greatly reduces the background noise of fluorescent signal such that a clear image of fluorescent beads can be taken using an ordinary epi-fluorescence microscope. Moreover, since all the fluorescent beads are in the same plane, images of fluorescent beads with overlapped areas can be joined together by comparing the local features of overlapped areas. This means that surface displacement in a large area can be tracked and the traction force of a large colony can be measured. Bead images with overlapped areas were taken using Olympus IX73 microscopy with installed manual micropositioning stage (Semprex, CA) and were merged into one large image via an ImageJ plugin (Fiji, http://fiji.sc/Image_Stitching).

**Finite element analysis of the intercellular tension.** The intercellular tension within a cell colony can be calculated following the monolayer stress microscopy[8, 9], which is an approach to map the stresses exerted between a cell and its neighbors from the measured traction force. The geometries of the cell colonies were first digitalized. Then we measured the cell traction force from the traction force microscopy and converted the traction force at the boundary layers into the body force. The cell colonies are regarded as linear elastic, isotropic material, with the Young's modulus and Poisson's ratio taken from literature[10]. The balance equation, compatibility equation and the Hooke's law together furnish a 2D mechanics boundary value problem that can be solved by the finite element package ABAQUS to obtain the intercellular tension. Finite element method (FEM) is an extensively used numerical technique to obtain an approximate solution of partial differential equations that are difficult to solve analytically.

## Supplementary results

**Video S1.** Real-time video of cell dispersion from a cohesive HCT-8 colony.

**Dispersion in colonies of different sizes.** Dispersion behavior was observed when HCT-8 cells were cultured on stiff hydrogels. On the stiff gels, dispersion in smaller colonies occurred statistically earlier than in larger colonies. Dispersion in colonies of different size on 20.7 kPa hydrogels is shown in Fig. S1.

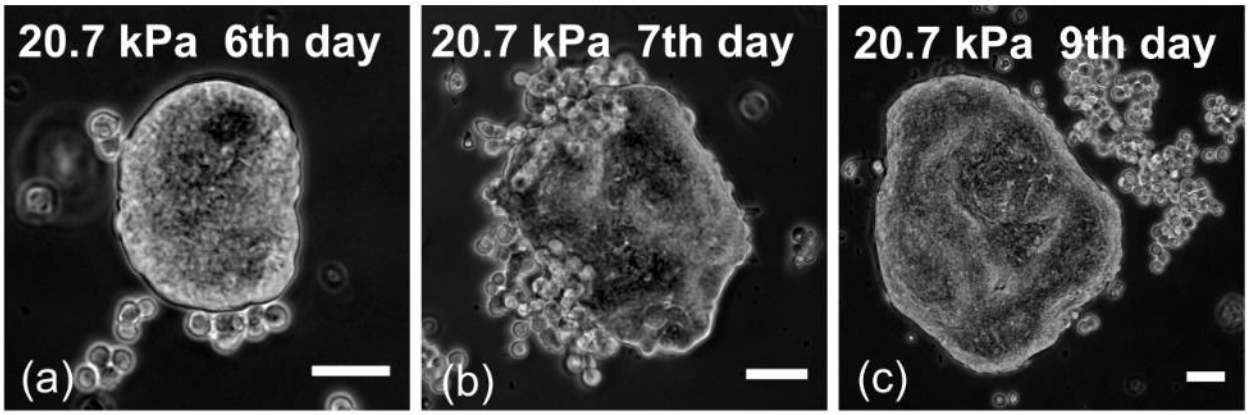


**Fig. S1.** (a-c) Dispersion of HCT-8 colonies of different size on 20.7 kPa gels. Scale bar: 50 μm.

**Phenotypic change and reduced E-cadherin expression level in dispersed HCT-8 cells.** Dispersion of the cell colonies was accompanied by the phenotypic change of the cells. The pre-dispersed cells exhibited regular epithelial morphology (Fig. S2a) with normal nuclei (Fig. S2c and S1e), whereas the dispersed cells exhibited rounded morphology (Fig. S2b) and abnormal nuclei (Fig. S1d and S1f). The boundaries of the nuclei of the pre-dispersed cells are smooth (Fig. S2c and S1e), whereas those of the dispersed cells are kinky (Fig. S2d and S1f). The circularity of pre-dispersed cell nuclei is larger than that of dispersed cell nuclei (Fig. S2g). The abnormality of cancer cell nuclei may result from altered packing of chromosomes[11]. The dispersed cells resemble the invasive phenotype of metastatic cancer cells[12].

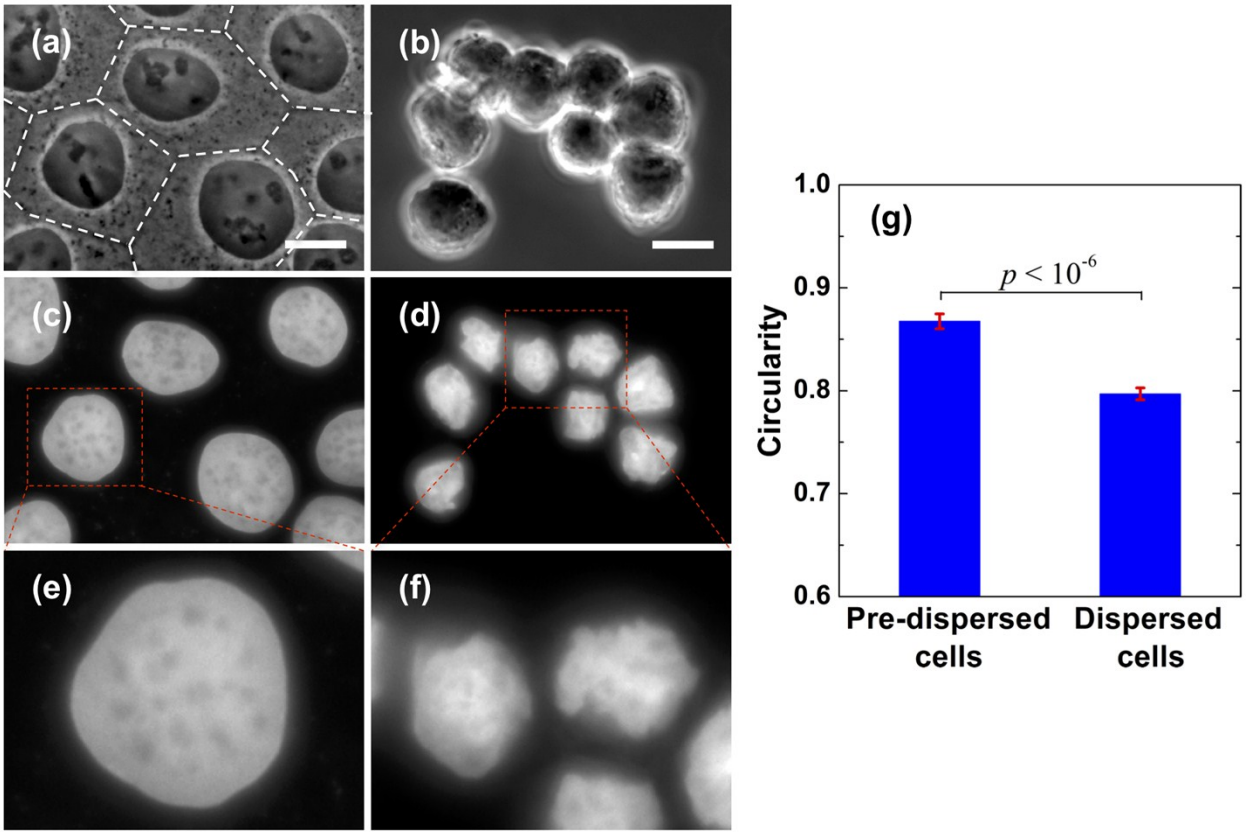


**Fig. S2.** Phase-contrast and nuclei staining images of pre-dispersed cells and dispersed cells. (**a**, **c** and **e**) The pre-dispersed cells exhibit regular epithelial morphology (**a**) with normal nuclei (**c** and **e**). (**b**, **d** and **f**) The dispersed cells exhibit rounded morphology (**b**) with abnormally shaped nuclei (**d** and **f**). (g) Circularity of nuclei of pre-dispersed and dispersed cells. Scale bar: 10 μm.

E-cadherin, the most abundant adhesion molecules in adherens junctions of epithelium, is a well-documented cancer suppressor[13]. Down-regulated E-cadherin expression has been widely found in metastatic cancer cells and is considered as a hallmark of metastasis[14, 15]. Immunofluorescent staining shows that pre-dispersed cells with regular epithelial morphology (Fig. S3a) adhere with neighbors tightly and E-cadherin concentrates along cell-cell borders (Fig. S3c). This pattern is disrupted in dispersed cells (collected from 20.7kPa gels with prolonged culture time, and recultured on the glass substrate), as displayed in Fig. S3d. The fluorescent signal of E-cadherin at cell-cell borders of the dispersed cells is more than 2-fold weaker, as shown in Fig. S3e. The reduced E-cadherin expression indicates that the dispersed cells have undergone a metastatic-like phenotypic change. On the other hand, we have stained both non-dispersing and dispersing HCT-8 cells cultured on PAA gels in a previous study, in which dispersed cells also displayed round morphology and lower E-cadherin expression[3]. It thus can be concluded that round morphology

and lower E-cadherin expression are specific to dispersed cells, not to pre-dispersed cells nor non-dispersing cells.

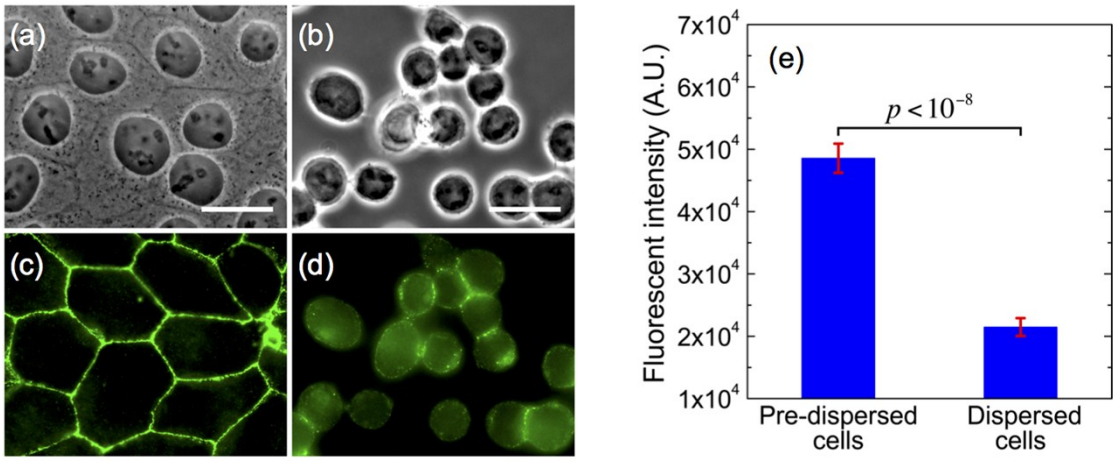


**Fig. S3**. The phenotypic change and the expression level of E-cadherin in the pre-dispersed and dispersed HCT-8 cells on glass substrates at day 2 of culture. Dispersed HCT-8 cells were collected from hydrogels with prolonged culture time and recultured on glass substrates. (**a** and **b**) Phase-contrast images of (**a**) pre-dispersed cells and (**b**) dispersed cells. (**c** and **d**) E-cadherin staining of (**c**) pre-dispersed cells and (**d**) dispersed cells. (**e**) Fluorescent intensity of E-cadherin at cell-cell borders of pre-dispersed cells and dispersed cells. Scale bar: 20 μm.

**Live/dead staining of dispersed HCT-8 cells.** Dispersed HCT-8 cells were first collected from stiff hydrogels with prolonged culture time and then re-cultured on glass substrate for live/dead staining. Staining images (Fig. S4) show that majority of the re-cultured dispersed HCT-8 cells were alive.

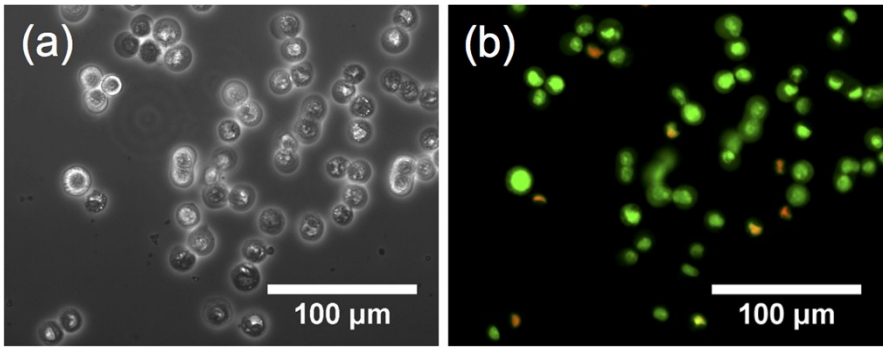


**Fig. S4.** Live/dead staining of dispersed HCT-8 cells. (**a**) Phase contrast and (**b**) live/dead staining of dispersed HCT-8 cells. Green represents alive cells, while red indicates dead cells.

**Cells at the interior of the colonies spread more than those at the boundary layers.** We observed that cells at the interior of the colonies spread more than those at the boundary layers (Fig. S5 a and b). The measured nuclei spread area of cells at the interior of the colonies is about 1.7 times larger than that of cells at the boundary layer (Fig. S5c).

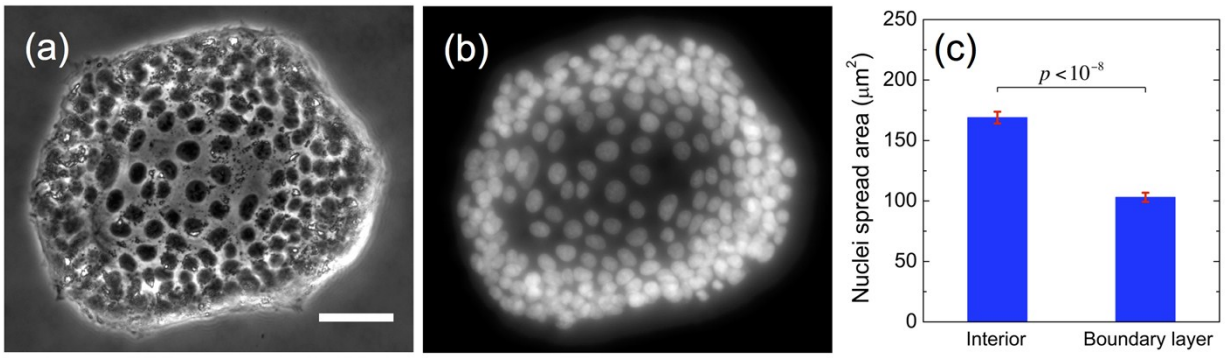


**Fig. S5.** Cell spreading at the interior and the boundary layers of the colony. (**a**) Phase contrast and (**b**) nuclei staining of one HCT-8 colony on 20.7 kPa gel. (**c**) Nuclei spread area of HCT-8 cells at the interior and at the boundary layer of colonies on 20.7 kPa. Scale bar: 50 μm.

**Comparison between the radial component and the tangential component of traction force.** For cell colonies with high circularity, we decompose the in-plane traction force into the radial ($T_r$) and tangential ($T_\theta$) components (Figs. S6 a-c). We notice that $|T_r| >> |T_\theta|$ in the boundary layer.

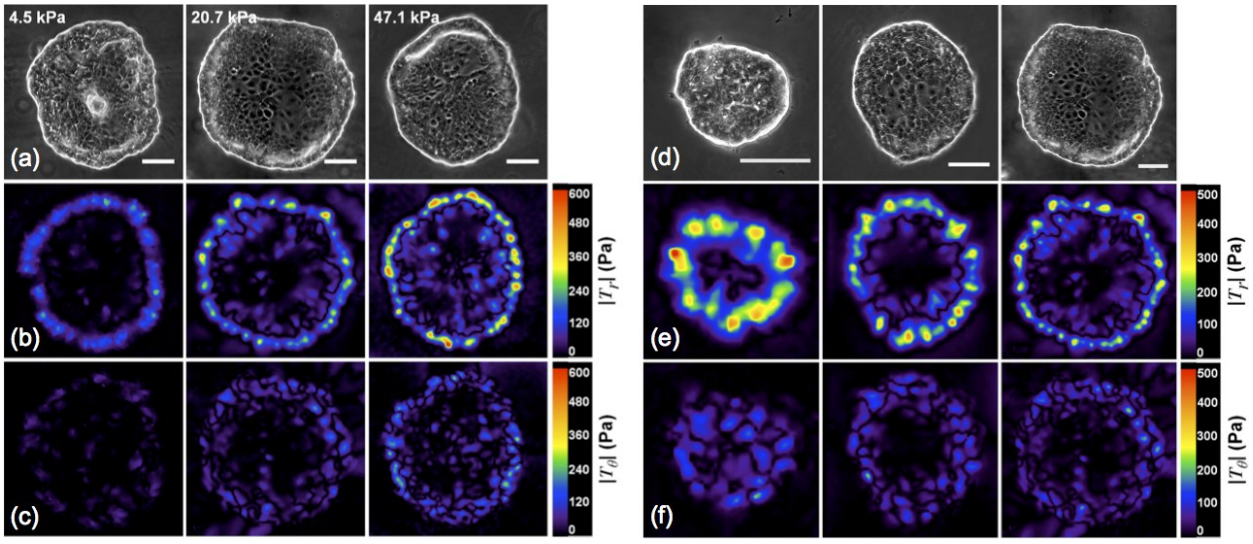


**Fig. S6.** Comparison between the radial component and the tangential component of traction force. (**a-c**) Traction force distribution of colonies at day 2 of culture on gels with different stiffness (4.5 kPa, 20.7 kPa and 47.1 kPa): (**a**) phase contrast, (**b**) radial component ($T_\theta$) and (**c**) tangential component ($T_\theta$) of the traction force. (**d-f**) Traction force distribution of colonies at day 2 of culture on 20.7 kPa gels with different size: (**d**) phase contrast, (**e**) radial component and

(**f**) tangential component of the traction force. Scale bar: 100 μm. The radial component of the traction force is much larger than the tangential component.

**3D confocal imaging of HCT-8 colonies.** To obtain the 3D profile of HCT-8 colonies, actin and nuclei of HCT-8 cells were stained and imaged using 3D confocal microscopy. On substrates (2.6 kPa, 20.7 kPa and 47.1 kPa) used in the experiments, the HCT-8 colonies at the boundary layer are slightly thicker than that at the interior (Fig. S7). This will not change the mechanical landscape using monolayer stress microscopy (MSM) calculations for which we simplify the colonies as an elastic material with homogeneous thickness, since our calculations are essentially based on the Newton's 2nd law in the continuum sense.

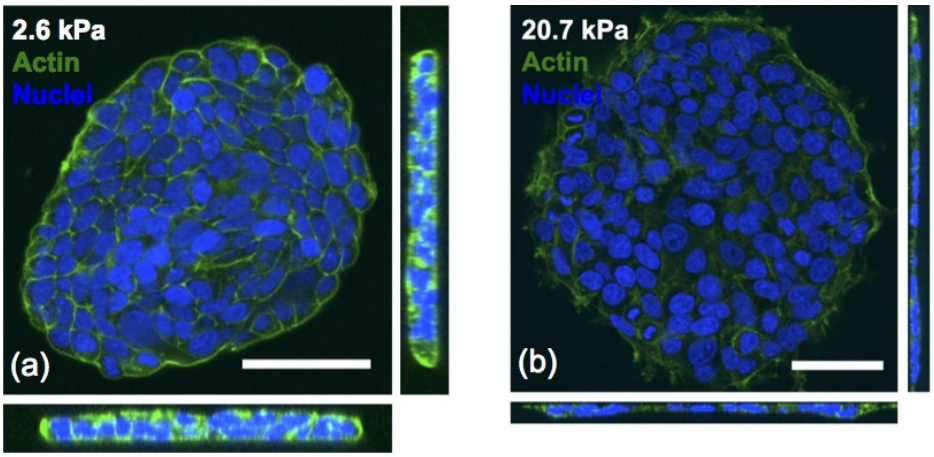


**Fig. S7.** 3D confocal imaging of actin and nuclei of HCT-8 colonies at day 2 of culture on (**a**) 2.6 kPa hydrogels and (**b**) 20.7 kPa hydrogels. Scale bar: 50 μm.

**Temporal traction force evolution of HCT-8 colonies treated with 6 μM blebbistatin at day 1 of culture time on 20.7 kPa gels.** Blebbistatin treatment at day 1 of culture time lowered HCT-8 colony traction and inhibited the dispersion behavior on 20.7 kPa gels. The relatively low traction force was maintained and the colonies remained cohesive for prolonged culture time. There are no statistically significant differences in the maximum traction and average traction at the boundary layer as the culture time went on (Fig. S8).

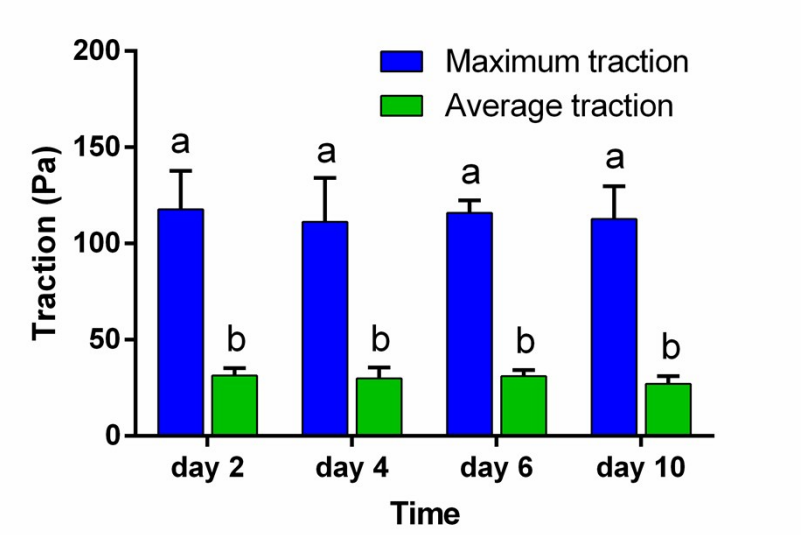


**Fig. S8.** Temporal traction force evolution of HCT-8 colonies treated with 6 μM blebbistatin at day 1 of culture time on 20.7 kPa gels. Two-way ANOVA (α=0.05) with Tukey's post-hoc test was employed for analysis. Error bars denote standard error of the mean (n≥10).

**Dynamic changes in the intracellular level of FAKpY397 in the cohesive HCT-8 colonies on 2.6 kPa and 47.1 kPa hydrogels .** Focal adhesion kinase (FAK), a focal adhesion-associated protein kinase, plays a key role in cell adhesion, spreading, and migration. FAK has been identified as a necessary molecule for the invasive behaviors in breast cancer cells[16]. The activated FAK phosphorylated at Tyrosine 397 (FAKpY397) positively correlates with integrin clustering, focal adhesion maturation, and cytoskeletal reinforcement[17]. It not only enhances growth factor-dependent mitogen-activated protein kinase activation but also increases the potential for malignant potential increase [18]. Interestingly, we found that FAKpY397 detected by immunofluorescent staining concentrates along the boundary region of the colonies within around a thirty-micron range (Fig. S9a), which is coincident with the traction force distribution (Fig. 2d). This phenomenon is more obvious on stiff hydrogels (47.1 kPa) at day 4 and day 8. Within the boundary region, the measured fluorescence intensities show that the intracellular levels of FAKpY397 in cells on stiff hydrogels (47.1 kPa) are significantly higher than those on soft hydrogels (2.6 kPa) (Fig. S9 b-d). On stiff hydrogels, the FAKpY397 levels are also higher in small colonies than those in large colonies (Fig. S9 b-d). This indicates that both substrate stiffness and colony size influence the intracellular levels of FAKpY397 in cohesive HCT-8 colonies, which resembles how substrate stiffness and colony size affect traction force

distribution. These results imply that cellular traction force is associated with FAK activation, which may play an important role in the malignant behaviors.

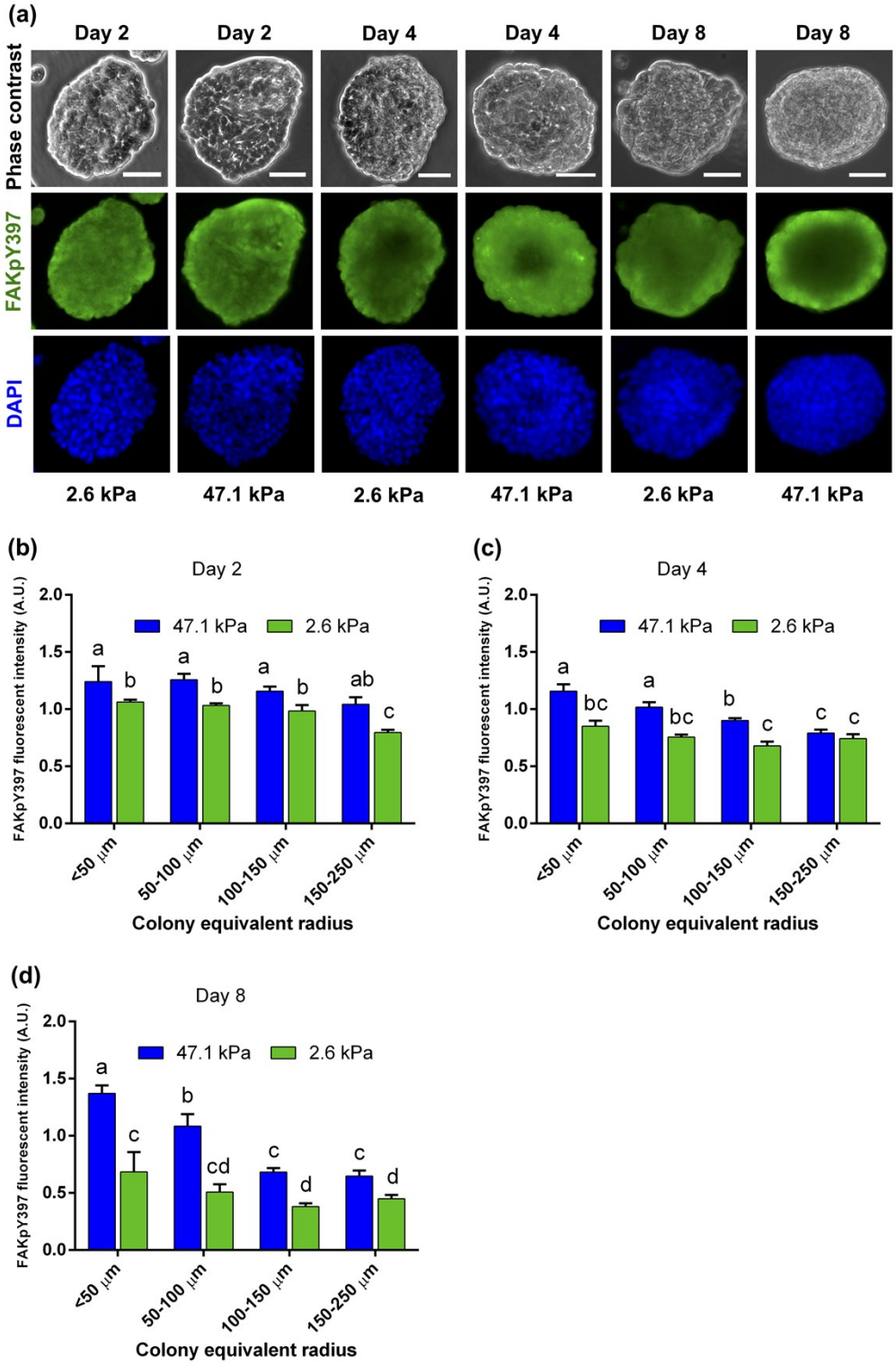

**Fig. S9.** Dynamic changes in the intracellular level of FAKpY397 in the cohesive HCT-8 colonies on 2.6 kPa and 47.1 kPa hydrogels. (**a**) Bright field and fluorescence images of HCT-8 colonies at different days on soft and stiff gels. Scale bar: 50 μm. Green: FAKpY397 stained with corresponding primary and secondary antibodies. Blue: nuclei stained with DAPI. FAKpY397 levels are high along the boundary of the colonies within around a thirty-micron range. (**b-d**) Quantification of the fluorescence intensities within the boundary region. The fluorescence intensities, which were normalized by cell numbers within the same region, show that substrate stiffness significantly affects the activation of FAK. Colony size effect is also statistically analyzed in the stiff gels at day 4 and day 8. Two-way ANOVA ($\alpha$=0.05) with Tukey's post-hoc test was employed for analysis. Error bars denote standard error of the mean. Any two groups with a common letter are not significantly different, while any two groups without a common letter are significantly different.

## References


1. Y.-L. Wang and R. J. Pelham, *Methods Enzymol.*, 1998, **298**, 489-496.
2. J. R. Tse and A. J. Engler, in *Curr. Protoc. Cell Biol.*, John Wiley & Sons, Inc., 2001.
3. X. Tang, T. B. Kuhlenschmidt, J. Zhou, P. Bell, F. Wang, M. S. Kuhlenschmidt and T. A. Saif, *Biophys. J.*, 2010, **99**, 2460-2469.
4. L. D. Landau, E. M. Lifshitz, J. B. Sykes, W. H. Reid and E. H. Dill, *Theory of Elasticity: Vol. 7 of Course of Theoretical Physics*, Physics Today, 1960.
5. J.-C. Wang and J.-S. Lin, *Biomech. Model. Mechanobiol.*, 2007, **6**, 361-371.
6. U. S. Schwarz, N. Q. Balaban, D. Riveline, A. Bershadsky, B. Geiger and S. A. Safran, *Biophys. J.*, 2002, **83**, 1380-1394.
7. Q. Tseng, E. Duchemin-Pelletier, A. Deshiere, M. Balland, H. Guillou, O. Filhol and M. Théry, *Proc. Natl. Acad. Sci. U. S. A.*, 2012, **109**, 1506-1511.
8. D. T. Tambe, C. Corey Hardin, T. E. Angelini, K. Rajendran, C. Y. Park, X. Serra-Picamal, E. H. Zhou, M. H. Zaman, J. P. Butler, D. A. Weitz, J. J. Fredberg and X. Trepat, *Nature Mater.*, 2011, **10**, 469-475.
9. D. T. Tambe, U. Croutelle, X. Trepat, C. Y. Park, J. H. Kim, E. Millet, J. P. Butler and J. J. Fredberg, *PLoS ONE*, 2013, **8**, e55172.
10. A. F. Mertz, S. Banerjee, Y. Che, G. K. German, Y. Xu, C. Hyland, M. C. Marchetti, V. Horsley and E. R. Dufresne, *Phys. Rev. Lett.*, 2012, **108**, 198101.
11. D. Gisselsson, J. Björk, M. Höglund, F. Mertens, P. Dal Cin, M. Åkerman and N. Mandahl, *Am. J. Pathol.*, 2001, **158**, 199-206.
12. G. A. Pihan, A. Purohit, J. Wallace, H. Knecht, B. Woda, P. Quesenberry and S. J. Doxsey, *Cancer Res.*, 1998, **58**, 3974-3985.
13. I. R. G. Beavon, *Eur. J. Cancer*, 2000, **36**, 1607-1620.
14. J. Yang, S. A. Mani, J. L. Donaher, S. Ramaswamy, R. A. Itzykson, C. Come, P. Savagner, I. Gitelman, A. Richardson and R. A. Weinberg, *Cell*, 2004, **117**, 927-939.
15. G. Handschuh, S. Candidus, B. Luber, U. Reich, C. Schott, S. Oswald, H. Becke, P. Hutzler, W. Birchmeier, H. Höfler and K. F. Becker, *Oncogene*, 1999, **18**, 4301-4312.
16. K. T. Chan, C. L. Cortesio and A. Huttenlocher, *J. Cell Biol.*, 2009, **185**, 357-370.

17. D. T. Butcher, T. Alliston and V. M. Weaver, *Nature Rev. Cancer*, 2009, **9**, 108-122.
18. M. J. Paszek, N. Zahir, K. R. Johnson, J. N. Lakins, G. I. Rozenberg, A. Gefen, C. A. Reinhart-King, S. S. Margulies, M. Dembo, D. Boettiger, D. A. Hammer and V. M. Weaver, *Cancer Cell*, 2005, **8**, 241-254.